

Electron-Like Fermi Surface and Remnant $(\pi,0)$ Feature in Overdoped $\text{La}_{1.78}\text{Sr}_{0.22}\text{CuO}_4$

T. Yoshida¹, X. J. Zhou², M. Nakamura³, S. A. Kellar², P. V. Bogdanov², E. D. Lu⁴, A. Lanzara^{2,4}, Z. Hussain⁴, A. Ino⁵, T. Mizokawa⁶, A. Fujimori^{1,6}, H. Eisaki², C. Kim², Z.-X. Shen², T. Kakeshita⁷, S. Uchida⁷

¹*Department of Physics, University of Tokyo, Bunkyo-ku, Tokyo 113-0033, Japan*

²*Department of Applied Physics and Stanford Synchrotron Radiation Laboratory, Stanford University, Stanford, CA 94305*

³*Department of Physics, Nara University of Education, Takabatake-cho, Nara 630-8523, Japan*

⁴*Advanced Light Source, Lawrence Berkeley National Lab, Berkeley, CA 94720*

⁵*Synchrotron Radiation Research Center, Japan Atomic Energy Research Institute, SPring-8, Mikazuki, Sayo, Hyogo 679-5198, Japan*

⁶*Department of Complexity Science and Engineering, University of Tokyo, Bunkyo-ku, Tokyo 113-0033, Japan*

⁷*Department of Advanced Materials Science, University of Tokyo, Bunkyo-ku, Tokyo 113-8656, Japan*

(October 31, 2018)

We have performed an angle-resolved photoemission study of overdoped $\text{La}_{1.78}\text{Sr}_{0.22}\text{CuO}_4$, and have observed sharp nodal quasiparticle peaks in the second Brillouin zone that are comparable to data from $\text{Bi}_2\text{Sr}_2\text{CaCu}_2\text{O}_{8+\delta}$. The data analysis using energy distribution curves, momentum distribution curves and intensity maps all show evidence of an electron-like Fermi surface, which is well explained by band structure calculations. Evidence for many-body effects are also found in the substantial spectral weight remaining below the Fermi level around $(\pi,0)$, where the band is predicted to lie above E_F .

PACS numbers: 74.25.Jb, 71.18.+y, 74.72.Dn, 79.60.Bm

Studies of low lying excitations and the Fermi surface in the high temperature superconductors by angle resolved photoemission spectroscopy (ARPES) have mostly been focused on $\text{Bi}_2\text{Sr}_2\text{CaCu}_2\text{O}_{8+\delta}$ (BSCCO)¹⁻⁶ and $\text{YBa}_2\text{Cu}_3\text{O}_{7-y}$ (YBCO)⁷. In these systems, however, additional features derived from complicated crystal structures, such as the Bi-O superstructures in BSCCO and the Cu-O chains in YBCO, have made the analysis rather complicated. In particular, the Bi-O superstructure complicates the interpretation of spectra around $(\pi,0)$, resulting in the controversy over the Fermi surface geometry¹⁻⁶. $\text{La}_{2-x}\text{Sr}_x\text{CuO}_4$ (LSCO), by virtue of the absence of these effects and the availability of high quality single crystal samples over the entire doping range, provides the opportunity to advance our understanding of the high temperature superconductors. In the underdoped regime, earlier studies have uncovered the presence of two electronic components⁸⁻¹⁰, a systematic suppression of the spectral weight near $(\pi/2, \pi/2)$ (when compared with that of overdoped samples or BSCCO for data taken under the same conditions), and straight Fermi surface segments near $(\pi,0)$ of width $\sim \pi/2$ ^{11,12}, which have been interpreted as evidence for electronic inhomogeneities. In the overdoped regime, an electron-like Fermi surface was observed in the high- T_c superconductors for the first time⁸, but despite this progress, important problems remain. Since ARPES data from underdoped samples are very broad, worries about the sample quality persist. There are also questions about the effects of the photoemission matrix element¹³, which makes it difficult to extract quantitative information about stripe effects on nodal spectral weight by comparing the experiments and theoretical calculations that

predict suppression¹⁴⁻¹⁶. We address these important questions by performing a detailed study of overdoped LSCO ($x=0.22$) where the stripe effects are expected to be weak, and have the aid of reliable band structure calculations (unlike the case of BSCCO). We performed ARPES in three Brillouin zones (BZ) and performed numerical simulations to investigate the matrix element effects. In the second BZ, using a favorable polarization, we have identified a sharp spectral feature along the diagonal direction in this sample that is comparable to that of BSCCO. This observation demonstrates that the surface quality of LSCO is comparable to that of BSCCO and gives credence to LSCO data in the underdoped region, since the sample quality of LSCO in the underdoped region is expected to be improved with decreasing Sr content. Our detailed analysis shows that the compound has an electron-like Fermi surface with additional spectral weight near $(\pi,0)$, which is the remnant of the flat band feature in the underdoped samples. The detailed comparison of experiment and simulation also provides a better understanding of the matrix element effect in these experiments.

The ARPES measurements were carried out at BL10.0.1.1 of the Advanced Light Source, using incident photons with an energy of 55.5 eV. We used a SCIENTA SES-200 spectrometer in angle mode, where one can collect spectra over ~ 14 degrees, corresponding to a momentum width of $\sim 1.1\pi$ (in units of $1/a$, where $a \sim 3.8\text{\AA}$ is the lattice constant). The total energy and momentum resolution was about 20 meV and 0.02π , respectively. We studied high quality single crystals of LSCO with $x=0.22$ grown by the traveling-solvent floating-zone method. The measurements were performed in an

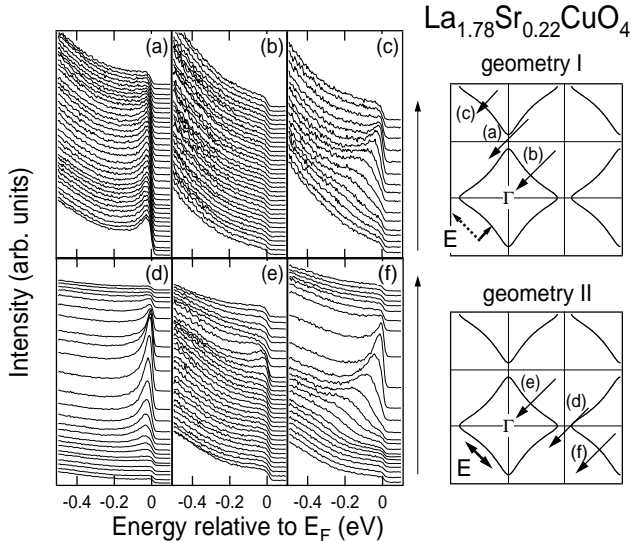


FIG. 1. Energy distribution curves for $\text{La}_{1.78}\text{Sr}_{0.22}\text{CuO}_4$ at 20 K. Right panels show the momentum space for each cut and the E-vector in the two geometries. For details, see the text.

ultra high vacuum of 10^{-11} Torr at 20 K and the samples were cleaved *in situ*. The position of the Fermi level (E_F) was calibrated with gold spectra.

Figure 1 shows energy distribution curves (EDC's) for two different experimental geometries along the directions shown in the right panel. In both geometries, the light is incident to the surface with an incident angle of $\sim 7^\circ$. The EDC's in geometry I were measured by rotating the sample, which causes the changes in the in-plane E -vector of the incident photons as shown in the right panel. On the other hand, in geometry II, the spectra were measured by moving the analyzer, and therefore the in-plane E -vector is fixed. While in geometry I, the E -vector was almost normal to the sample surface, resulting in a small in-plane E component, in the geometry II, the E -vector was almost parallel to the sample surface. Panels (a) and (d) show ARPES spectra around the $(\pi, 0)$ point. These spectra show a single peak with little dispersion, which will be addressed in the discussion below as a remnant of the "flat band" feature appearing below E_F even for $x < 0.2^8$. Panels (b) and (e) give the nodal cut [(0,0) to (π, π) direction] in the first BZ for each geometry. One can see that panel (e) shows a dispersive feature while panel (b) shows almost no corresponding spectral feature, due to transition matrix element effects. Thus, compared to the previous results, we could observe the nodal feature in the first BZ more clearly in geometry II. Furthermore, as shown in panels (c) and (f), we found that the nodal state feature become stronger in the second BZ, particularly in geometry II. As a whole, geometry II gives clearer dispersive features, probably because the in-plane E -vector is much larger than that in geometry I. These results show that

there are significant matrix element effects which should be carefully considered in order to extract intrinsic information. It should be emphasized that the intensity of the first BZ nodal state in underdoped LSCO is still much weaker than that in BSCCO or overdoped LSCO observed under the same experimental conditions. These relative changes in data with doping under the same experimental geometry are intrinsic but the matrix element effect makes quantitative analysis more difficult.

One may suspect that the weak dispersion of the features in underdoped LSCO, particularly in the nodal direction⁹, may be due to inferior surface quality (roughness, defects etc.). The present results have shown that the sharpness of the nodal feature seen in geometry II is comparable to that in BSCCO, which demonstrates the high quality of the LSCO surfaces. One can expect that the sample quality decreases with increasing x because of the disorder introduced by Sr and the difficulty in the crystal growth due to the Sr solubility limit. In fact, underdoped samples give better cleavage than overdoped samples, which possibly indicates the better surface quality for the underdoped samples. Therefore, the ARPES results in the underdoped region, which show broad features around $(\pi, 0)$ and interpreted as a two-component feature⁹, should be reliable results.

The band dispersions along the $(0,0)$ to $(\pi, 0)$ and $(0,0)$ to (π, π) directions, which have been derived from the ARPES spectra by taking the second derivatives, are shown in Fig. 2. In going from $(0,0)$ to $(\pi, 0)$, the band reaches E_F at $k_x \sim 0.8\pi$ but substantial spectral weight remains below E_F up to $(\pi, 0)$. However, as shown in the inset, the peak in the momentum distribution curves (MDC's) clearly crosses the Fermi level around $(0.85\pi, 0)$ concomitant with the decrease of spectral weight for $k_x > 0.85\pi$. This behavior is not seen in optimally-doped and underdoped LSCO along the $(0,0)$ - $(\pi, 0)$ line⁸. The LDA band calculation also predicts an electron like Fermi surface for $x \geq 0.17^{17,18}$, although the calculation shows finite band dispersions along the c -axis and the Fermi surface is somewhat k_z -dependent. The k_z dispersion is expected to be strongly renormalized in real materials¹⁹. Therefore, we state that the $x = 0.22$ has an electron-like Fermi surface centered at $(0,0)$. The red line shows a tight-binding fit to the experimental band dispersion with parameters $E_p - E_d = 1.2$ eV, $t_{pd\sigma} = 0.5$ eV, $E_{xy} \equiv t_{pp\sigma}/2 - t_{pp\pi}/2 = 0.15$ eV. Here, $t_{pd\sigma}$ and E_{xy} are the transfer integrals for the nearest-neighbor O $2p_\sigma$ -Cu $3d_{x^2-y^2}$ and O $2p_x$ -O $2p_y$ overlap, respectively. The best fit values for $t_{pd\sigma}$ and E_{xy} are much smaller than those obtained from a tight-binding fit to the LDA band-structure calculation²⁰ due to the band narrowing corresponding to the mass enhancement by a factor of ~ 3 in the overdoped region²¹.

Figure 3 shows the spectral weight plot integrated over a 30 meV window around the Fermi level [(a),(c)] for both geometries and simulations of the spectral weight plot for each geometry including transition matrix element effects [(b),(d)] (see below). Integrating over the nar-

row window of the order of the energy resolution makes it possible to obtain the spectral weight at E_F , which approximately represents the Fermi surface. The Fermi surfaces at $k_z = 0$ and π/c from the band-structure calculation for $\text{La}_{2-x}\text{M}_x\text{CuO}_4$ ($x = 0.2$)¹⁷, as well as the Fermi surface from the present tight-binding fit are superimposed on Fig. 3(a). As a whole, they well describe the global features related to the Fermi surface obtained from ARPES. In particular, looking at the nodal direction in the second BZ, they agree well with each other. The volume enclosed by the tight-binding Fermi surface is $S_{FS} \simeq 0.8 \times 2\pi^2$, which satisfies Luttinger's sum rule [$S_{FS} = 2\pi^2(1-x)$] within experimental accuracy.

Here, we have performed simulations of spectral weight distribution including matrix-element effects by using the same method described in^{22,23}. The simulation method which we apply here has given a good account of the photoemission results on graphite²² and TaSe_2 ²³. Therefore, this is a good starting point to understand the matrix element effect in the present ARPES results, at least qualitatively. First, we consider the initial state $|i\rangle = (1/\sqrt{N}) \sum_{i,j} e^{-iq \cdot (R_j + \tau_i)} a_i \phi_i(r - R_j - \tau_i)$ as the two-dimensional tight-binding ground state, where ϕ_i is the atomic orbital Cu $3d_{x^2-y^2}$ or O $2p_x, p_y$. The matrix element factor is given by $M(\mathbf{k}) = |a_{d_{x^2-y^2}} A_{d_{x^2-y^2}} + a_{p_x} A_{p_x} + a_{p_y} A_{p_y}|^2$, where $A_{d_{x^2-y^2}}, A_{p_y}, A_{p_x}$ are angular distribution factor from each atomic orbital Cu $3d_{x^2-y^2}$, and O $2p_x, p_y$ ²⁴. a_d, a_{p_x} , and a_{p_y} have been determined from the tight-binding fit to the dispersion of ARPES result as shown in Fig. 2. The spectral function $A(\mathbf{k}, \omega)$ of the tight-binding band was approximated by broadening the δ -function with width of ω^2 , where ω is in units of eV. Then, the simulated momentum distribution of spectral weight is given by $n(\mathbf{k}) = M(\mathbf{k}) \int I(\mathbf{k}, \omega) d\omega$, where $I(\mathbf{k}, \omega)$ is spectral weight broadened by energy resolution of 20 meV.

As shown in Fig. 3(b), in geometry I, the nodal states in the first BZ show almost no spectral weight while those in second BZ are enhanced, consistent with the experimental data in Fig. 3(a). This implies that the suppression in geometry I compared to geometry II is caused by

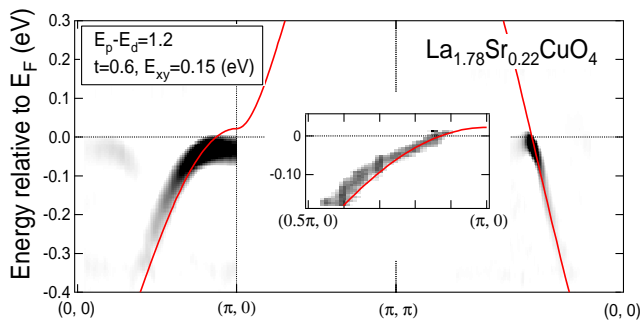


FIG. 2. Energy dispersion and a tight-binding fit for $\text{La}_{1.78}\text{Sr}_{0.22}\text{CuO}_4$. The gray plot in the inset was obtained by normalizing the spectra to the peak in each MDC.

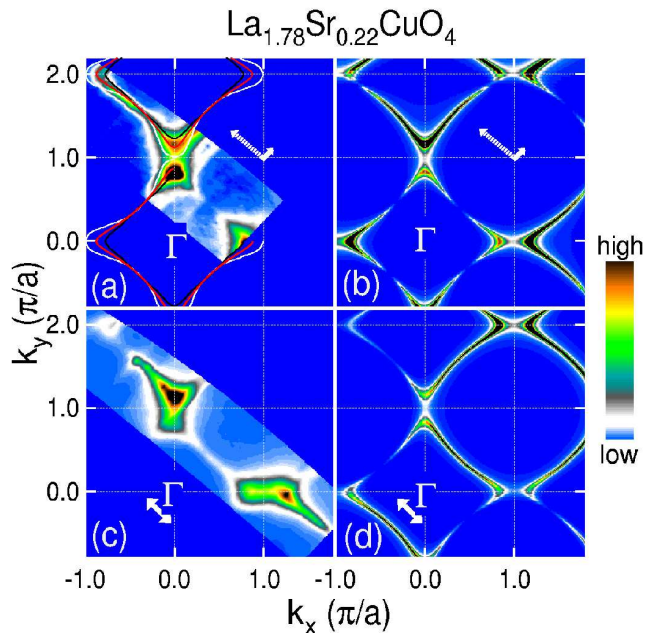


FIG. 3. Spectral weight integrated within 30 meV of the Fermi level. White arrows designate the E vector. (a)(c); Experiment. (b)(d); Simulation. White and black curves in (a) represent the Fermi surfaces of band calculation¹⁷ at $k_z = 0$ and π/c , respectively, and red curves represents the Fermi surface from the present tight-binding fit. Note that the spectral weight in the nodal direction is enhanced for geometry II [(c) and (d)] compared to geometry I [(a) and (b)].

matrix element effects. According to the simulation, the smaller matrix elements in the first BZ are a result of the combination of the symmetry of the $d_{x^2-y^2}$ orbital and the large out of plane component in the E -vector. The enhancement in the second BZ may be caused by the angular distribution factor of the three atomic orbitals, because they have a small emission probability for small angles when the E -vector is vertical to the surface. In geometry II, we can see the clear dispersion and spectral weight in the nodal state in the first BZ as shown in Fig. 1(e) and Fig. 3(c). The simulation in Fig. 3(d) shows an enhancement of the spectral weight in the $(0,0)$ - (π, π) direction compared to the nodal states of the first BZ in geometry I, which qualitatively agrees with the experimental results.

While the overall features in the experimental results agree with the simulation as shown above, there was still a discrepancy between them regarding the spectral weight distribution near $(\pi, 0)$. Here, we discuss the possible origin of the strong spectral weight around the $(\pi, 0)$ point which cannot be described within the simple two dimensional electron-like Fermi surface picture. As shown in Fig. 4, the spectral weight distribution around $(\pi, 0)$ shows a relatively straight contour along the k_x direction, which is slightly narrower than that in Nd-LSCO ($|k_y| < \pi/4$)¹¹. This spectral weight distribution is very similar to that of the flat band which appears be-

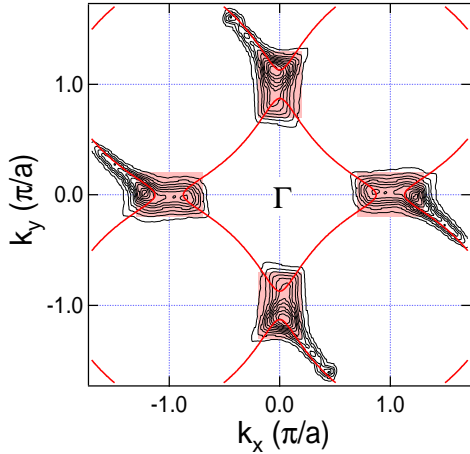


FIG. 4. Contour plot of the spectral weight shown in Fig. 3(c) symmetrized with respect to the Γ point. Red curves show the electron-like Fermi surface obtained from the fit to the experiment as shown in Fig. 2. Shaded regions around $(\pi,0)$ reflect a remnant of the “flat band”.

low E_F for smaller x . Presumably the $(\pi,0)$ flat band feature which exists in the optimum and underdoped regions does not completely lose its spectral weight even for $x = 0.22$ (and probably for $x = 0.3$, see data in Ref.⁸) where the saddle point is located above E_F . Therefore, the spectral weight around $(\pi,0)$ appears as a remnant of the “flat band”. Recently, there have been debates as to whether there exists an electron-like Fermi surface in BSCCO or not¹⁻⁶. While this discussion has been complicated by the Bi-O superstructures, the present results from overdoped LSCO clearly shows an electron-like Fermi surface with much less ambiguity. One may suspect that the matrix element may suppress spectral weight only around the $(\pi,0)$ point making the hole-like Fermi surface appear electron-like. However, as far as the matrix element simulation using the simple tight-binding scheme is concerned, such a suppression localized in momentum space around $(\pi,0)$ is difficult to explain. This is consistent with an earlier calculation¹³. In the case of BSCCO, the possibility of additional states at $(\pi,0)$ has been proposed¹. In the present case, strong intensity around $(\pi,0)$, which is not predicted by the simulation, always exists irrespective of polarization geometries, while the nodal states are strongly affected by matrix element effects. This implies an intrinsic unusual electronic structure such as stripes associated with the “flat band” feature.

As seen in Fig. 4, we have shown that the electronic structure of LSCO with $x = 0.22$ shows two features. One is the nodal Fermi surface which is found to be consistent with the band structure calculation. The other is the remnant flat band which gives rise to a straight segment of spectral weight near the $(\pi,0)$ region. These two features are qualitatively similar to those observed in Nd-LSCO and LSCO with $x = 0.15$ samples^{11,12}, al-

though quantitatively the flat band effect in LSCO with $x = 0.22$ is weaker. This dual nature of the electronic structure can be explained in terms of order-disorder stripes competition¹². The origin of the nodal state can be understood by considering strongly disordered stripes and/or weakened stripe order. In the latter case, one may begin to recover the underlying band structure. The underlying electronic structure will manifest itself stronger as the charge ordering effect becomes weaker in LSCO with $x = 0.22$.

In conclusion, we have unambiguously observed an electron-like Fermi surface in slightly overdoped LSCO with $x = 0.22$, which agrees with the band-structure calculation. By utilizing the matrix element effects, we have obtained clear dispersion and sharp peak features for the nodal states comparable to BSCCO. The transition matrix element effects have been discussed by simulations, which account for the enhancement in the second BZ and for different geometries. Although the stripe effect in the present sample is weaker, the observation of the nodal spectral weight and the straight segment near $(\pi,0)$ is consistent with the picture of order-disorder competition of stripes in the system.

This work was supported by a Grant-in-Aid for Scientific Research “Novel Quantum Phenomena in Transition Metal Oxides”, a Special Coordination Fund from the Science and Technology Agency and the New Energy and Industrial Technology Development Organization (NEDO). Advanced Light Source of Lawrence Berkeley National Laboratory is operated by U.S. Department of Energy’s Office of Basic Energy Science, Division of Material Science.

-
- ¹ Y.-D. Chuang, A. D. Gromko, D. S. Dessau, Y. Aiura, Y. Yamaguchi, K. Oka, A. J. Arko, J. Joyce, H. Eisaki, S. I. Uchida, K. Nakamura, and Yoichi Ando, Phys. Rev. Lett. **83**, 3717 (1999).
 - ² D.L. Feng, W.J. Zheng, K.M. Shen, D.H. Lu, F. Ronning, J.-I. Shimoyama, K. Kishio, G. Gu, D. Van der Marel, Z.-X. Shen, cond-mat/9908056.
 - ³ P. V. Bogdanov, A. Lanzara, X. J. Zhou, S. A. Kellar, D. L. Feng, E. D. Lu, J.-I. Shimoyama, K. Kishio, Z. Hussain, Z. X. Shen, cond-mat/0005394.
 - ⁴ A.D. Gromko, Y.-D. Chuang, D.S. Dessau, K. Nakamura, and Yoichi Ando, cond-mat/0003017.
 - ⁵ H. M. Fretwell, A. Kaminski, J. Mesot, J. C. Campuzano, M. R. Norman, M. Randeria, T. Sato, R. Gatt, T. Takahashi, and K. Kadowaki, Phys. Rev. Lett. **84**, 4449 (2000).
 - ⁶ S. V. Borisenko, M. S. Golden, S. Legner, T. Pichler, C. Durr, M. Knupfer, J. Fink, G. Yang, S. Abell, H. Berger, Phys. Rev. Lett. **84**, 4453 (2000).
 - ⁷ M. C. Schabel, C.-H. Park, A. Matsuura, Z.-X. Shen, D. A. Bonn, R. Liang, and W. N. Hardy, Phys. Rev. B **B57**, 6107 (1998).

- ⁸ A. Ino, C. Kim, T. Mizokawa, Z.-X. Shen, A. Fujimori, M. Takaba, K. Tamasaku, H. Eisaki and S. Uchida, *J. Phys. Soc. Jpn.* **68**, 1496 (1999).
- ⁹ A. Ino, C. Kim, M. Nakamura, T. Yoshida, T. Mizokawa, Z.-X. Shen, A. Fujimori, T. Kakeshita, H. Eisaki, and S. Uchida, *Phys. Rev. B* **B62**, 4137 (2000).
- ¹⁰ A. Ino, C. Kim, M. Nakamura, T. Yoshida, T. Mizokawa, Z.-X. Shen, A. Fujimori, T. Kakeshita, H. Eisaki, S. Uchida, *cond-mat/0005370*.
- ¹¹ X. J. Zhou, P. Bogdanov, S. A. Kellar, T. Noda, H. Eisaki, S. Uchida, Z. Hussain, and Z.-X. Shen, *Science* **286** 268 (1999).
- ¹² X. J. Zhou, T. Yoshida, S. A. Kellar, P. V. Bogdanov, E. D. Lu, A. Lanzara, M. Nakamura, T. Noda, T. Kakeshita, H. Eisaki, S. Uchida, A. Fujimori, Z. Hussain, and Z.-X. Shen, *cond-mat/0009002*.
- ¹³ A. Bansil and M. Lindroos, *Phys. Rev. Lett.* **83**, 5154 (1999).
- ¹⁴ T. Tohyama, S. Nagai, Y. Shibata, and S. Maekawa, *Phys. Rev. Lett.* **82**, 4910 (1999).
- ¹⁵ M. Fleck, A. I. Lichtenstein, E. Pavarini and A. M. Oles, *Phys. Rev. Lett.* **84**, 4962 (2000).
- ¹⁶ M. Ichioka and K. Machida, *J. Phys. Soc. Jpn.* **68**, 4020 (1999).
- ¹⁷ J.-H. Xu, T. J. Watson-Yang, J. Yu, and A. J. Freeman, *Phys. Lett. A* **120**, 489 (1987).
- ¹⁸ W. E. Pickett, *Rev. Mod. Phys.* **61**, 433 (1989).
- ¹⁹ K. Tamasaku, T. Ito, H. Takagi, and S. Uchida, *Phys. Rev. Lett.* **72**, 3088 (1994).
- ²⁰ M. S. Hybertsen, M. Schluter and N. E. Christensen, *Phys. Rev. B* **39**, 9028 (1989).
- ²¹ A. Ino, T. Mizokawa, K. Kobayashi, A. Fujimori, T. Sasagawa, T. Kimura, K. Kishio, K. Tamasaku, H. Eisaki, and S. Uchida, *Phys. Rev. Lett.* **81**, 2124 (1998).
- ²² H. Daimon, S. Imada, H. Nishimoto, and S. Suga, *J. Electron Spectrosc. Relat. Phenom.* **76**, 487 (1995).
- ²³ T. Matsushita, S. Imada, H. Daimon, T. Okuda, K. Yamaguchi, H. Miyagi, and S. Suga, *Phys. Rev. B* **56**, 7687 (1998).
- ²⁴ S. M. Goldberg, C. S. Fadley and S. Kono, *J. Electron Spectrosc. Relat. Phenom.* **21**, 285 (1981).